Published online 27 August 2013 *Nucleic Acids Research, 2013, Vol. 41, No. 22* ***10529–10541***
doi:10.1093/nar/gkt748

Structural insights into VirB-DNA complexes reveal mechanism of transcriptional activation of virulence genes

Xiaopan Gao[1], Tingting Zou[1], Zhixia Mu[1], Bo Qin[1], Jian Yang[1], Sandro Waltersperger[2], Meitian Wang[2], Sheng Cui[1,*] and Qi Jin[1,*]

[1]MOH Key Laboratory of Systems Biology of Pathogens, Institute of Pathogen Biology, Chinese Academy of Medical Sciences & Peking Union Medical College, No.9 Dong Dan San Tiao, Beijing 100730, P.R. China and [2]PX Beamlines Swiss Light Source at Paul Scherrer Institute, CH-5232 Villigen, Switzerland

Received May 10, 2013; Revised July 27, 2013; Accepted July 29, 2013

ABSTRACT

VirB activates transcription of virulence genes in *Shigella flexneri* by alleviating heat-stable nucleoid-structuring protein-mediated promoter repression. VirB is unrelated to the conventional transcriptional regulators, but homologous to the plasmid partitioning proteins. We determined the crystal structures of VirB HTH domain bound by the *cis*-acting site containing the inverted repeat, revealing that the VirB-DNA complex is related to ParB-ParS-like complexes, presenting an example that a ParB-like protein acts exclusively in transcriptional regulation. The HTH domain of VirB docks DNA major groove and provides multiple contacts to backbone and bases, in which the only specific base readout is mediated by R167. VirB only recognizes one half site of the inverted repeats containing the most matches to the consensus for VirB binding. The binding of VirB induces DNA conformational changes and introduces a bend at an invariant A-tract segment in the *cis*-acting site, suggesting a role of DNA remodeling. VirB exhibits positive cooperativity in DNA binding that is contributed by the C-terminal domain facilitating VirB oligomerization. The isolated HTH domain only confers partial DNA specificity. Additional determinants for sequence specificity may reside in N- or C-terminal domains. Collectively, our findings support and extend a previously proposed model for relieving heat-stable nucleoid-structuring protein-mediated repression by VirB.

INTRODUCTION

The pathogenic bacterium evolves from its harmless ancestor through the acquisition of the virulence genes located on plasmids, bacteriophages or pathogenic islands (1). The expression of the virulence genes enables the microbe to survive in new host environment. The evolution of *Shigella* from the innocuous *Escherichia coli* represents a good example for the understanding of how the acquired virulence genes contribute to pathogenic lifestyle of the bacterium. *Shigella* is the causative agent for bacillary dysentery, posing a leading public health concern worldwide (2,3). *Shigella* can be subdivided into four species, *Shigella flexneri*, *Shigella dysenteriae*, *Shigella sonnei* and *Shigella boydii*, in which most of the pathogenicity studies were carried out on the prevalent *S. flexneri*. The virulence of *S. flexneri* depends on the virulence genes clustered within the so called 'entry region', a 31-kb segment on the virulence plasmid (4,5). These genes encode a variety of proteins, including invasins mediating the invasion of intestinal epithelium, structural proteins forming the type III secretion system and the effector proteins (6). The vast quantity of the virulence genes products presents a great metabolic burden; therefore, their expressions are strictly controlled involving both the plasmid encoded regulatory system and the chromosome encoded global gene regulation network. When the growth conditions are not ideal for invasion, the transcription of the virulence genes is repressed by a chromosomally encoded heat-stable nucleoid-structuring protein (H-NS) (7). H-NS binds the AT-rich DNA segment near the promoters, from which H-NS spreads along the DNA, forming H-NS-DNA filaments or DNA-H-NS-DNA bridges (8,9). The resulting nucleoprotein structures function as the obstacles to impede the movements of RNA polymerase, thereby silent the

*To whom correspondence should be addressed. Tel: +86 10 67828669; Fax: +86 10 67855012; Email: cui.sheng@ipb.pumc.edu.cn
Correspondence may also be addressed to Qi Jin. Tel: +86 10 65105157; Fax: +86 10 65105160; Email: jinqi@ipbcams.ac.cn

The authors wish it to be known that, in their opinion, the first two authors should be regarded as Joint First Authors.

transcription (10,11). In response to proper environmental signals, i.e. pH value, temperature and osmolarity similar to the site of invasion (12), the H-NS-mediated transcriptional repression can be alleviated. A transcriptional cascade is then initiated with the activation of *virF* gene expressing an AraC-like protein VirF that in turn activates the transcription of the *virB* gene (13–15). The product VirB relieves the H-NS-mediated transcriptional repression, leading to the activation of many virulence genes (16).

VirB belongs to an unusual type of transcriptional activator because the protein does not recruit RNA polymerase, indicating an indirect transcriptional activation (17,18). Indeed, VirB shares little sequence homology with the conventional transcriptional regulators, but it is homologous to the plasmid partitioning proteins ParB, SopB and KorB (19–21). VirB-mediated transcriptional activation initiates with the recognition of the *cis*-acting sites upstream promoter. It was speculated that on the binding to the *cis*-acting site, VirB could destabilize and collapse the repressive H-NS-DNA complexes, releasing of the trapped RNA polymerase so that the transcription reactivates (17,22,23). However, the mechanism underlying the VirB-mediated promoter derepression remained elusive. Previous studies identified several *cis*-acting sites for VirB binding. A consensus [5′-(A/G)(A/T)G(G)AAAT-3′] was derived from the analyses of InvE (identical to VirB) binding sites upstream *icsB*, *spa15* and *virA* promoters in *S. sonnei* (24) and the VirB binding sites upstream the *icsB*, *icsP* and *virB* promoters in *S. flexneri* (17,23,25). The consensus shares the core elements with the A-boxes in ParS-like site targeted by the ParB-like proteins (21,26). Especially, the *cis*-acting sites upstream *icsB* and *icsP* promoters contain the inverted repeats similar to the A2-A3 boxes in ParS site (21).

The investigation of VirB–DNA interaction is the key to elucidate of the function of VirB. Similar to many sequence specific DNA-binding proteins, VirB binds DNA nonspecifically *in vitro* (22,27), whereas the recognition of the specific DNA sequence by VirB is essential for transcriptional activation *in vivo* (24). Mutations at the VirB binding site could lead to the complete loss of VirB-mediated promoter activation (17,25). However, the structural basis for the DNA sequence specificity is unavailable.

MATERIALS AND METHODS

Construction of plasmids

To construct plasmids encoding VirB variants and mutants, the XhoI-EcoRI fragment was generated by PCR and inserted into pBAD-mychis (Invitrogen). Point mutations were introduced using site-directed mutagenesis (QuickChange™). The icsP promoter (a 1256-bp fragment upstream of the icsP transcription start site) was amplified from the virulence plasmid pCP301 and combined to a promoterless *lacZ* gene and inserted into the lower-copy-number plasmid pACYC184 with BamHI and XbaI site. The sequences were verified by DNA sequencing.

Gene mutation by lambda red recombination

The virB gene knockout mutant strain was made by homologous recombination using the λ-red recombination system described previously (28). Briefly, the kanamycin resistance gene from pKD13 plasmid was amplified by PCR using primer pairs whose sequences are homologous to the 45 bp regions upstream and downstream of the *virB* gene. The PCR products were purified and transformed into electro-competent *S. flexneri 2a* strain 301 containing the red helper plasmid pKD46. The structure of *virB::kan* lesion was confirmed by PCR and DNA sequencing.

β-galactosidase assay

Transcription of the *LacZ* gene under the control of icsP was determined by measuring β-galactosidase activity in bacteria *S. flexneri 2a virB* knockout strain containing plasmids pACYC184 and pBAD-mychis expressing VirB variants and mutants as described previously (22). Assays were performed at least in triplicate, and the data are expressed as the mean of two independent measurements.

Protein expression, purification and crystallization

Plasmids encoding VirB variants VirB full length (FL) (1–309 aa), VirB delta N (129–309 aa), VirB delta C (1–250 aa) and VirB core (129–250 aa) or VirB mutants was transformed to Rosetta™ (DE3) competent cells (Novagen), respectively. The expression of the recombinant protein was induced by adding 0.5 mM IPTG when the culture reached OD_{600} ~1.0. The selenomethionine derivatives were obtained by inducing protein expression in *E. coli* strain B834 (DE3) grown in LeMASTER medium containing L-selenomethionine. The harvested bacteria cells were resuspended in lysis buffer containing 50 mM Tris–HCl (pH 7.0), 2 M NaCl and 30 mM imidazole and disrupted by ultrasonication. The protein purification is composed of three steps. The crude lysate were first loaded to Ni-NTA resin (invitrogen) and eluted with 200 mM imidazole. The eluate was further purified using Hitrap Q HP 5 ml of column (GE healthcase) with the linear gradient of 150–1000 mM NaCl. The polishing step of the purification was the size exclusion chromatography using Superdex 75 HR 10/30 column (GE Healthcare) equilibrated with 20 mM Tris–HCl (pH 7.0), 150 mM NaCl and 2 mM DTT. To crystallize VirB core/DNA complexes, multiple oligonucleotides (23–33 bp) containing the *cis*-acting sites identified upstream icsP or icsB promoters were synthesized, annealed with their complementary stands and then mixed with VirB core (12 mg/ml) at molar ratio DNA:protein = 2:1, respectively. The mixtures were incubated on ice for 2 h to allow the assembly of the nucleoprotein complexes before the crystallization trials. Only icsB-wt and icsP-wt (Supplementary Table S1) co-crystallized with VirB core. The crystal containing Set-Met labeled VirB core and 5-bromouracil (5-BRU) incorporated icsB-wt was obtained by mixing 0.8 μl of sample with 1 μl of reservoir buffer containing 0.1 M $MgCl_2$, 0.1 M Sodium Acetate

pH = 4.5, 22% PEG400, 3% dimethyl sulfoxide (v/v) in a vapor diffusion system at 22°C. The crystals containing native VirB core/icsB-wt and VirB core/icsP-wt were obtained using the similar approaches, except the reservoir buffer was optimized to 0.1 M $MgCl_2$, 0.1 M Sodium Acetate pH 4.3, 30% PEG400, 8% 1,3-Butanediol (v/v) and 0.1 M $MgCl_2$ 0.1 M Sodium acetate pH 4.5, 16% PEG400, respectively. The cryocooling of the crystals were carried out by the soaking in reservoir buffer containing 10% ethylene glycol 30–60 s before the flash freezing in liquid nitrogen.

Structure determination

Highly redundant single anomalous dispersion data to 2.42 Å on crystals containing Se-Met labeled VirB core/5-BRU incorporated icsB-wt and data to 2.78 Å on the crystals containing native VirB core/icsP-wt were collected at beamline X06DA SLS PSI (Villigen, Switzerland). Data to 2.43 Å on crystals containing native VirB core/icsB-wt were collected at beamline BL17U at SSRF (Shanghai, China). The data sets were integrated and scaled using XDS package. The space group identified for icsB-wt containing crystals was $P2_12_12$; for icsP-wt containing crystals was C2. One VirB core and one dsDNA (icsB-wt or icsP-wt) are present in the asymmetric unit. Programs SHLEX C/D/E were used to locate the heavy atoms (one selenium on VirB core and two bromines on icsB-wt) and to calculate the initial phases, leading to an interpretable electron density map. The manual model building was carried out by using the program Coot. The structures of the native VirB core/icsB-wt and VirB core/icsP-wt were solved by molecular replacement (Phaser, CCP4 package) using the structures of Se-Met labeled VirB core and 5-BRU incorporated icsB-wt as the searching models. Refinement of all structures were performed by using PHENIX, which included bulk solvent correction, individual B factor refinement, simulated annealing and anomalous f′ and f″ refinement. Data collection and model statistics are summarized in Table 1.

Fluorescence and anisotropy measurement

Fluorescence anisotropy experiments were performed with a Fluoromax-4 fluorimeter (HORIBA Jobin Yvon), equipped with a Glan-Thompson prism polarizer. Briefly, 1.4 ml of buffer [50 mM Tris–HCl (pH 7.5), 150 mM NaCl] containing 4 nM fluorescently labeled DNA FAM-icsB-wt-50 bp (SangonBiotech Shanghai Co., Ltd, Supplementary Table S1) was pre-equilibrated in a quartz cuvette at 15°C;. Protein samples were added stepwise. After 3 min equilibration, the anisotropy data were collected using an excitation wavelength of 493 nm and monitoring the emission at 518 nm. The band pass was 3 nm for excitation and 3 nm for emission. A maximum number of 10 trials were performed until <2% deviation of the signal was reached.

Electrophoretic mobility shift assays

To prepare the probe for electrophoretic mobility shift assay (EMSA), the synthetic DNA icsB-wt was 5′-labeled using [^{32}P]γ- ATP (5000 Ci/mmol, Furui Biotech, Beijing, China) and purified using G-25 MicroSpin columns (GE healthcare). VirB variants (2 μM), labeled icsB-wt (2 nM), unlabeled competitor DNA (icsB-wt or icsB-mut supplied in 2×, 4×, 8×, 16×, 32× and 64× excess of VirB variant) were mixed. The mixtures were incubated at room temperature in the binding buffer containing 20 mM Tris–HCl (pH 8.0), 50 mM NaCl, 5 mM $MgCl_2$, 5% glycerol (w/v), 10 ng/ml poly dI-dC and 0.1 mg/ml bovine serum albumin for 30 min. The resulting samples were resolved on 6% native PAGE in 0.5 × TBE buffer at 20 V/cm for ~1 h. The gels were visualized with Typhoon Trio Variable Mode Imager (GE healthcare).

Molecular weight determination by size-exclusion chromatography

Superdex 75 10/300GL column (GE healthcare) was equilibrated with the buffer containing 50 mM Tris–HCl (pH 8.0) and 100 mM NaCl, and calibrated using molecular weight standards, γ-globulin (158 kDa), ovalbumin (45 kDa), myoglobin (17 kDa) and vitamin B12 (1.35 kDa). The purified VirB variants (~1 mg/ml) were loaded to the column running at the flow rate of 0.15 ml/min.

RESULTS

The mode of DNA binding by VirB

To investigate the molecular determinants underlying the DNA binding, we analyzed the DNA binding properties of VirB and a set of truncations (Figure 1A). We tested the full-length protein, denoted 'VirB FL', the truncation lacking C-terminal (1–250 aa), denoted 'VirB delta C', the truncation lacking N-terminal (129–309 aa), denoted 'VirB delta N' and truncation lacking both C- and N-terminal (129–250 aa), denoted 'VirB Core'. All VirB variants were overexpressed in *Escherichia coli* and purified to high homogeneity. The 6xHIS tag was engineered at the N-terminal of each VirB variants to facilitate purification.

We performed the fluorescence anisotropy experiments to study the binding capability of VirB variants to a fluorescently labeled DNA FAM-icsB-wt-50 bp derived from the *cis*-acting site upstream *icsB* promoter (17). We observed the binding isotherms that could be fitted to the Hill equation (29). The data points of the four VirB variants were fitted to the curves with the coefficients of determination (R^2) ranging from 0.94 to 0.99, respectively, indicating the good fittings to the Hill equation (Figure 1B). VirB FL binds the DNA with an apparent dissociation constant K_d of 11 ± 0.3 nM. Lacking the N-terminal portion did not affected the DNA-binding capabilities significantly, whereas lacking the C-terminal portion accounted for >10-fold loss of DNA-binding affinities because VirB delta N binds DNA with a K_d of 12 ± 0.3 nM, and VirB delta C binds DNA with a K_d of 139 ± 15 nM. VirB core harboring a putative HTH motif binds the DNA with slightly lower affinity (K_d = 16 ± 3 nM) comparing the VirB FL and VirB delta N. The aforementioned results demonstrate that although the C-terminal portion is important to the

Table 1. Data collection and refinement statistics

Parameter	VirB core (SeMet derivative)/ icsb (DNA with 5-BRU modifications) (PDB ID: 3VWB)	VirB core/ icsb (native DNA) (PDB ID: 3W3C)	VirB core/ icsp (native DNA) (PDB ID: 3W2A)
Data collection			
Space group	$P2_12_12$	$P2_12_12$	C2
Cell dimensions			
a, b, c (Å)	57.32, 163.05, 39.57	56.14, 163.40, 39.67	176.32, 39.83, 73.49
α,β,γ (°)	90.00, 90.00, 90.00	90.00, 90.00, 90.00	90.00, 90.00, 90.00
X ray source	SLS BEAMLINE X06DA	SSRF BEAMLINE BL17U	SLS BEAMLINE X06DA
Wavelength (Å)	0.9792 (Se peak)	1.54001	0.9796 (Se peak)
Data range (Å)	46.89-2.42	40.85-2.43	48.25-2.78
Reflections unique	27467	13931	23902
R_{sym}[a] (last shell)	0.067 (0.768)	0.049 (0.254)	0.090 (0.761)
$I/\sigma I$	21.56 (2.43)	20.49 (4.77)	12.86 (2.31)
Completeness (%) (last shell)	99.8 (98.8)	96.6 (95.8)	98.1 (89.2)
Redundancy (last shell)	7.77 (7.54)	4.95 (3.97)	6.68 (5.76)
Refinement			
Resolution range (Å)	46.89–2.42	40.85–2.43	48.25–2.78
Reflections (non-anomalous), cut-off, cross validation	27 362 (14 781), F>1.99, 1358	13 893 (13 893), F>1.88, 694	23 902 (12 578), F>2.0, 1194
R_{work}[b]/R_{free}[c] (last shell)	0.2370/0.2710 (0.3640/0.3901)	0.2640/0.2797 (0.3532/0.3778	0.2415/0.2624 (0.4199/0.4428)
Atoms			
Non-hydrogen protein atoms	2053	2061	1904
Protein	903	931	920
DNA	1088	1060	943
Solvent	62	70	41
B-factors average ($Å^{2)}$	65.76	60.1	96.03
Protein ($Å^2$)	53.25	48.9	74.13
DNA ($Å^2$)	77.39	71.3	118.99
Solvent ($Å^2$)	43.32	41.0	59.59
r.m.s.d			
Bond lengths (Å)	0.004	0.003	0.004
Bond angles (°)	0.979	0.749	0.924
Validation			
MolProbity score	2.11, 90th percentile[d]	1.76, 98th percentile[d]	2.44, 93rd percentile[d]
Clashscore, all atoms	14.36	7.79	18.7
% Poor rotamers	1.90	1.90	1.94
% residues in favored regions, allowed regions, outliers in Ramachandran plot	96.5, 2.6, 0.9	97.4, 0.9, 1.75	92.9, 6.2, 0.9

[a]$R_{sym} = \sum_{hkl}\sum_j |I_{hkl,j} - I_{hkl}|/\sum_{hkl}\sum_j I_{hkl,j}$, where I_{hkl} is the average of symmetry-related observations of a unique reflection.
[b]$R_{work} = \sum_{hkl} ||F_{obs}(hkl)|-|F_{calc}(hkl)||/\sum_{hkl}|F_{obs}(hkl)|$.
[c]R_{free} = the cross-validation *R* factor for 5% of reflections against which the model was not refined.
[d]100th percentile is the best among structures of comparable resolution; 0th percentile is the worst.

DNA-binding capability of VirB, the N-terminal portion of VirB negatively affected the overall DNA binding capability (specific and non-specific) of the HTH domain. A plausible explanation is that the N-terminal domain of VirB might block the DNA binding site of the HTH domain in the absence of the C-terminal domain. The fitting of the isotherms for DNA binding by VirB FL gave the hill coefficient n = 2.8, identifying a positively cooperative DNA binding (Figure 1B). The removal of the N-terminal of VirB seemed to further improve the cooperativity in DNA binding (the Hill coefficient for VirB delta N is n = 4.0), whereas the removal of C-terminal abolished entirely the cooperativity. Because VirB delta C and VirB core bind the DNA with the Hill coefficients of n = 1.0 and n = 0.9, respectively. These results suggest that the C-terminal portion of VirB is essential for cooperative DNA binding.

Crystallization and structure determination

To gain insights into VirB-DNA interaction, we carried out structural studies of various nucleoprotein complexes comprising VirB variants and a set of DNAs. We used the dynamic light scattering method to evaluate the qualities of the samples in solution, identified that only VirB core-DNA complex was monodispersed. We next prepared the nucleoprotein complexes by mixing VirB core with a number of DNA (23–33 bp) containing the *cis*-acting sites upstream virulence gene promoters. The DNA duplexes were blunt-ended or with the complementary

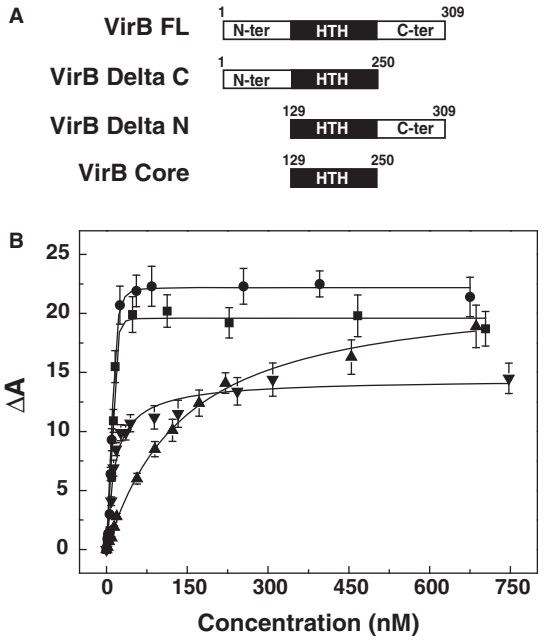

Figure 1. The mode DNA binding by VirB variants. (**A**) VirB variants used in this study. (**B**) Fluorescence anisotropy changes (ΔA) were recorded when titrating VirB FL (black circle), VirB delta N (black square), VirB delta C (black down-pointing triangle) or VirB core (black up-pointing triangle) into a solution containing fluorescently labeled FAM-icsB-wt-50 bp. The experimental points were fitted to the Hill equation: $\Delta A = \Delta A_{max} * [S]^n / (K_d{}^n + [S]^n)$, where ΔA is the fluorescence anisotropy changes, [S] is the concentration of the VirB variants and 'n' is the Hill coefficient. Non-linear regression against cooperative binding isotherms reveals dissociation constants (K_d) and Hill coefficients (n) of 11 ± 0.3 nM and 2.8 for VirB FL, 12 ± 0.3 nM and 4.0 for VirB delta N, 139 ± 15 nM and 1.0 for VirB delta C and 16 ± 3 nM and 0.9 for VirB core.

sticky ends. A 26 bp DNA 'icsB-wt' and a 31-bp DNA 'icsP-wt' (Supplementary Table S1) co-crystallized with VirB core. We first determined the crystal structure containing selenomethionine labeled VirB bound by the 5-BRU incorporated icsB-wt by single wavelength anomalous dispersion. The resulting model was then used as searching model to determine the crystal structures of native VirB core/icsB-wt and VirB core/icsP-wt complexes by molecular replacement. We could build 116 aa of 122 aa from VirB core, all 52 bp from icsB-wt and 46 bp of 62-bp from icsP-wt in the electron density maps. All crystals structures were finally refined to the atomic models with excellent refinement and stereochemistry qualities (Table 1).

Overall structure of VirB-DNA complex

The structures of VirB core from different crystal forms are identical. The structural comparison of gave the r.m.s.d. values of 0.87–0.95 Å over 116 Cα of VirB core. In the crystal structure of VirB core/icsB-wt, DNA duplexes with complementary 5′ overhangs are connected end-to-end, forming serpentine helix through the lattice. The engineered triple A and triple T overhangs are base paired at the junctures (Figure 2A). VirB core molecules connect the parallel DNA strands and align along the direction perpendicular to the DNA strands, providing additional contacts to stabilize the lattice. Similar packing was observed in VirB-icsP-wt crystals; however, there were insufficient electron densities to build the bases at the junctures.

VirB core comprises seven α-helices folding into the N- and C-terminal subdomains. The helices α2-α3 form a typical HTH DNA binding motif (22). Helices α4-α7 forms a distorted 4-helical bundle that is connected to the HTH motif by a linker (Figure 2B). In a search for structural relatives of VirB core in protein data bank (PDB) using DALI search tool (30), the significant hits are ParB-like proteins. VirB core is structurally related to the HTH domain of P1 plasmid ParB (Supplementary Figure S1), F plasmid SopB and RP4 plasmid KorB with the r.m.s.d. of 2.0, 2.7 and 4.0 for 113, 106 and 94 corresponding Cα, (Figure 2B and C).

VirB preferentially binds the box2 in the inverted repeats

Both DNA used for co-crystallization contained the inverted repeats, box1 and box2 (Figure 3A). The box2 of icsB-wt icsP-wt are identical (5′-ATGAAAT-3′) that match 7/8 positions at the consensus established previously (17,24,25). The box1 in icsB-wt (5′-ATGAAAC-3′) and the box1 icsP-wt (5′-CTGAAAT-3′) match 6/8 positions at the consensus sequence. In the crystal structures, VirB core only binds box2 containing with the best match to the consensus, whereas the box1 were unoccupied. The HTH motif of VirB docks in the major groove of the box2 in icsB-wt and icsP-wt in the similar way (Figure 3A); however, differences were also found. In general, the α3 of HTH motif presenting the 'recognition helix' is buried in the major groove (Figure 3B) with the helical axis running parallelly along the plane of the base. VirB core provides six contacts to the backbone phosphates of icsB-wt, four of which are clustered on one side of box2, two contacts on the other side. VirB core provides seven contacts to the backbone phosphates of icsP-wt, four of which are clustered on one side of box2, three others on the other side (Figure 3A). The asymmetric backbone recognition may be essential for the correct docking of VirB. It was previously shown that K152 and K164 of VirB are essential in DNA binding and transcriptional activation (22). Our crystal structure reveals the underlying structural basis. Nζ of K152 provides a tight salt bridge to Op2 of G_{8b} in icsB-wt (2.61 Å), and the backbone NH of K152 donates a hydrogen bond to Op2 of the adjacent T_{7b} (2.15 Å, 138°). Nζ of K164 provides another strong salt bridge (2.45 Å) to the Op2 atom of the phosphate backbone of T_{2c}. Additionally, we identified a number of other residues that also contribute to the DNA backbone recognition, including Y151, T166, Q170 and F190 (Figure 3A and B). Residues A161 and K194 contact the backbone of icsP-wt; however, the corresponding interactions are not observed in VirB core-icsB-wt complex.

VirB provides three base contacts to icsB-wt and two base contacts to icsP-wt (Figure 3A and B). In VirB core-icsB-wt complex, the side chain of R167 is oriented to

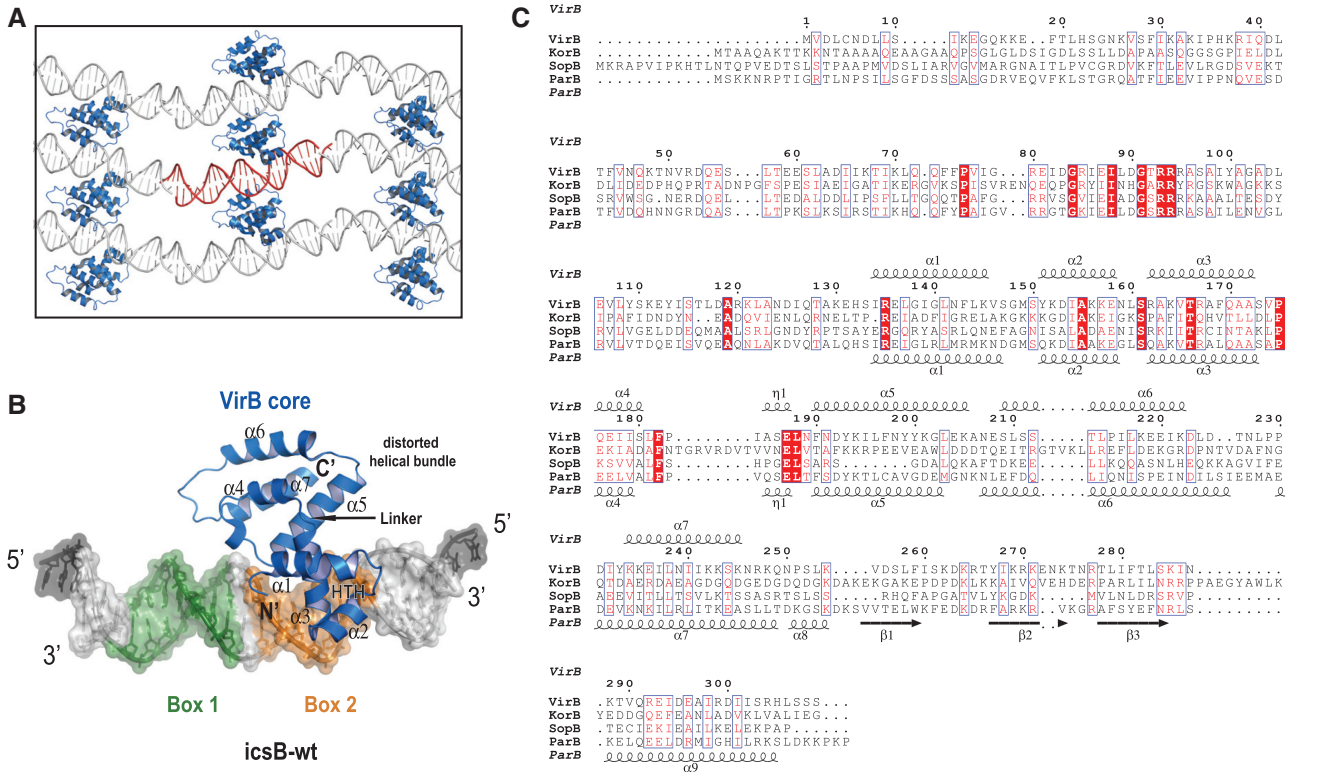

Figure 2. Overall structure of VirB core complexed by the inverted repeats. (**A**) View of crystal lattice of VirB core/icsB-wt complex. VirB core is highlighted in blue ribbon models. (**B**) Ribbon model of VirB core docking into the box2 of the inverted repeats upstream icsB promoter. Seven helices forming the N-terminal HTH motif, a linker and the C-terminal distorted helical bundle are labeled, respectively. The double-stranded DNA icsB-wt is shown with stick model with the calculated semitransparent surface, in which box2 is highlighted in orange, box1 is highlighted in green and the engineered 5′ triple dA is highlighted in black. (**C**) Structure-based multiple sequence alignment of the transcriptional regulator VirB and the plasmid partitioning proteins ParB, KorB and SopB. The secondary structure of VirB is shown on the top, whereas the secondary structure of ParB is shown at the bottom. Invariant residues among these proteins are highlighted with red background; conserved residues are shown in red.

donate two hydrogen bonds to G_{3c} base (R167 Nη2 – G_{3c} N7: 1.97Å, 167°; R167 Nη1 – G_{3c} O6: 2.77Å, 157°). The plane of the guanidinium is twisted with respect to the plane of guanine base of G_{3c} (dihedral angle ~24°) so that the side chain of R167 donate another hydrogen bond to the adjacent T_{4b} (R167 Nη2 – T_{4b} O4: 2.87 Å, 132°) (Figure 4A). R162 donates a hydrogen bond to the base of A_{7b} (2.14 Å, 125.5°). The plane of the guanidinium is nearly perpendicular to the plane of the adenosine base (dihedral angle ~99°) (Figure 4B). In VirB core-icsP-wt complex, R167 donates two hydrogen bonds to G_{3c} base (R167 Nη2 – G_{3c} N7: 2.10 Å, 167°; R167 Nη1 – G_{3c} O6: 2.03 Å, 160°). The twist angle between the planes of the guanidinium and the guanine base reduced to ~14°; thus, the side chain of R167 is out of the hydrogen bonding range to the T_{4b} (Figure 4C). R162 adopts a different side chain conformation to donate double hydrogen bonds to A_{7b} base (R162 Nη2 – A_{7b} N7: 2.70 Å, 143°; R162 Nη1 – A_{7b} C8: 2.73 Å, 158°) (Figure 4D). Residue A163 provides the third base contact to T_{5b} in icsB-wt. The corresponding contact was unavailable in VirB cor-icsP-wt complex.

The conformational changes of DNA on binding by VirB

In the crystal structure of VirB core-icsB-wt, there are sufficient electron densities to model all 52 base pairs of icsB-wt, and the DNA is associated with lower temperature factor than that of icsP-wt (Table 1). Therefore, we used VirB core/icsB-wt structure to study the conformation of the bound DNA. The double helix of icsB-wt is slightly bent on binding by VirB with the overall curvature (31) of ~22°. The bending occurs at the box2 because the duplex (C_{-10}-C_0) containing an unbound box1 is straight (overall bend angle ~5.5°; the average bend of the dinucleotide steps of box1 is 1.4°), whereas the duplex (A_1-C_{12}) containing the box2 is bent with the angle of ~24.0°. The averaged bend of the dinucleotide steps (A_4-T_7), an A-tract segment 'AAAT', is 3.3°, in contrast to the average bend of 1.5° for the rest base pair steps. In the crystal structure of P1 ParB-ParS complex, the A2 box (5′-TTGAAAT-3′) of ParS shares the most sequence homology with box2 of icsB-wt. The A2 box contains the identical A-tract segment 'AAAT'. Although the A2 box is docked by the HTH domain of ParB, it is not bent. The average bend of the dinucleotide steps of (A_7-T_4) of A2 box is 1.5°. These data suggest that the binding of VirB induces a bend at the A-tract segment of box2. The similar feature is not shared by ParB. Additionally, the box2 of icsB-wt exhibits the evident fluctuation of DNA minor groove width that is uncorrelated with appreciable changes in major groove width (Figure 5). Comparing with the standard B-form DNA, the minor grooves is

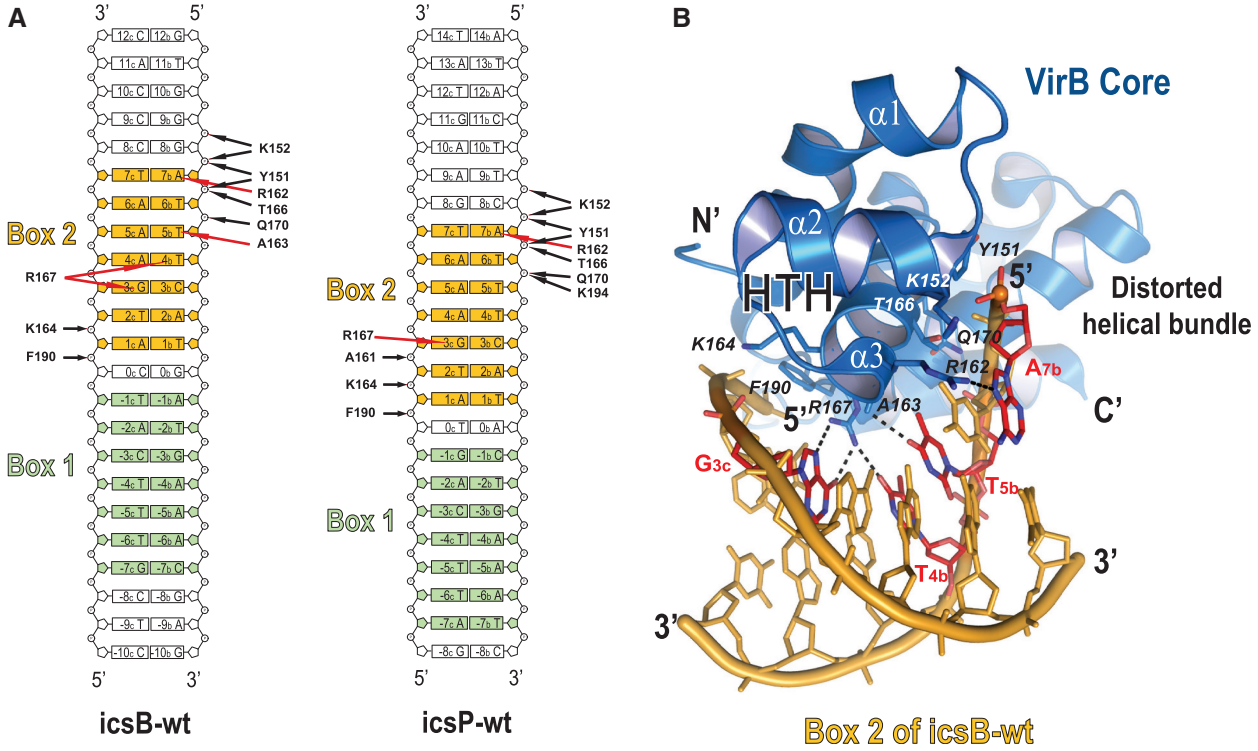

Figure 3. VirB-DNA contacts. (**A**) Ladder representations of VirB contacts to 26 bp DNA icsB-wt (left) and to icsP-wt (right) (only the nucleotides visible in the crystal structures are drawn). In stands b and c of icsB-wt and icsP-wt, the central base pair is numbered as 0; the base pairs one the box2 (orange) side are assigned to positive numbers and the base pairs on the box1 (green) side are assigned to negative numbers. Contacts to backbones are indicated with black arrows; contacts to bases are indicated with red arrows. (**B**) Contacts between HTH domain (blue) of VirB and box2 (orange) of icsB-wt. Residues involving the contacts are shown in stick model. Hydrogen bonds to the bases (red) are indicated with dashed lines.

wider at A_1-G_3 steps followed by the significant compression at A_4-T_7 steps. By contrast, the box1 of icsB-wt that is not bound by VirB does not exhibit the similar oscillation in minor groove width. In the structure of icsP-wt, we observed the similar oscillation in DNA minor groove widths in box2 where VirB is bound and in box1 where VirB is not bound (Figure 5). However, the box1 of icsP-wt is only partially visible in the electron density map, and this portion is associated with the highest temperature factor. Therefore, the geometry measured for box1 could be influenced by its flexibility.

VirB binds DNA specifically and nonspecifically

The crystallographic data supports that the box2 of the inverted repeats is preferentially recognized by VirB; therefore, we investigated the interplay between VirB and DNA by EMSA. We used a radioactively labeled icsB-wt as the probe and synthesized a mutant DNA in which the box2 'ATGAAAT' was replaced by 'GCTGGG C', denoted 'icsB-mut' (Supplementary Table S1) as the competitor. Such mutations have previously been shown to lead to defective VirB-mediated promoter activation (17). We also included poly dI-dC in EMSA buffer to eliminate non-specific interactions. We observed that when the protein concentration increased to 2 μM, the labeled DNA fully shifted with the VirB variants. VirB FL produced a shift of high-ordered complex with large size, which could barely enter the native PAGE (Figure 7A). However, this large complex did not seem to base on the specific DNA–protein interaction because the shifted band was efficiently competed with either unlabeled icsB-wt or icsB-mut. After the addition of the unlabeled DNA, we observed the enrichment of a predominate shift with smaller size. This band was only competed by icsB-wt, but not by icsB-mut, indicating a specific nucleoprotein complex. These results support our crystallographic findings that the box2 of the inverted repeat is the key sequence specifically recognized by VirB. Similarly, VirB delta N formed the large complex with icsB-wt, which could be competed by either icsB-wt or icsB-mut (Figure 7B). We observed a lower band after the addition of unlabeled DNA, which was competed by icsB-wt, but not by icsB-mut. VirB truncations lacking the C-terminal portion, VirB delta C and VirB core, did not produce the super-shift as observed for VirB FL and VirB delta N, suggesting that the C-terminal portion is responsible for the formation of the large nucleoprotein complex (Figure 7C and D). We observed a single shift produced by VirB delta C, which was competed by unlabeled icsB-wt but not by icsB-mut (Figure 7C). VirB core produced two shifts, suggesting that each box of the inverted repeats in icsB-wt may accommodate a HTH domain, although with different affinities. The double bands were efficiently competed with icsB-wt, but much less efficiently competed with icsB-mut (Figure 7D).

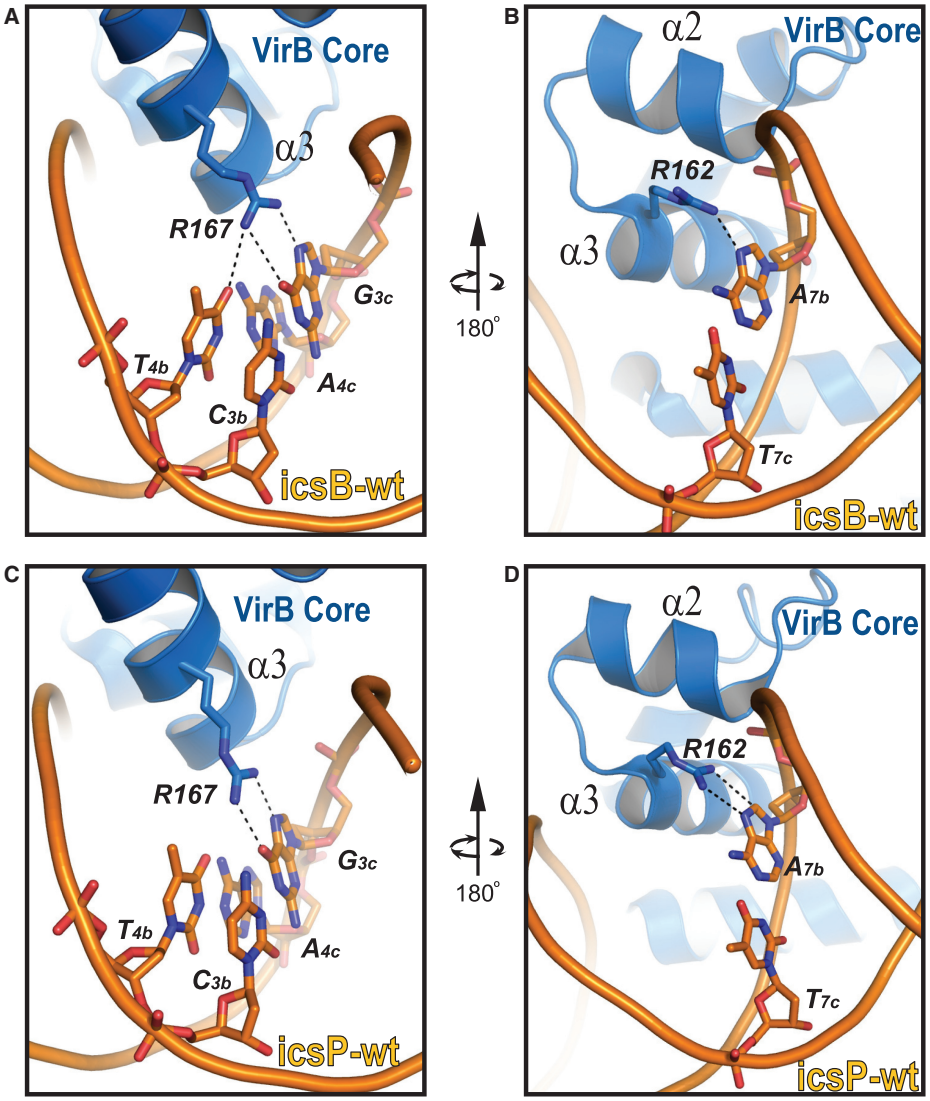

Figure 4. Base recognition by R167 and R162. (**A**) R167 reads bases G_{3c} and T_{4b} of box2 in icsB-wt. (**B**) R162 reads bases A_{7b} of box2 in icsB-wt. (**C**) R167 reads bases G_{3c} of box2 in icsP-wt. (**D**) R162 reads bases A_{7b} of box2 in icsP-wt. Residues (blue) involving the contacts are shown in stick model. Hydrogen bonds to the DNA bases (orange) are indicated with dashed lines.

The determinant for dimerization/oligomerization of VirB

It was previously proposed that the leucine zipper of VirB mediates the dimerization and the C-terminal domain of VirB mediates the high-ordered oligomerization (22). Our crystallographic study has ruled out the existence of leucine zipper domain and showed that the isolated HTH domain of VirB exists as monomers in crystal. To assess the molecular determinants for dimerization/oligomerization in solution, we carried out the size-exclusion experiments to determine the molecular weight of four VirB variants. As shown in Supplementary Figure S2, VirB variants with the C-terminal domain form dimer/oligomer in solution. The apparent molecular weight calculated for VirB FL was 99.2 kDa, which is close to the expected molecular weight of a VirB trimer (106.2 kDa). The molecular weight calculated for VirB delta N was 42.0 kDa, matching the expected molecular

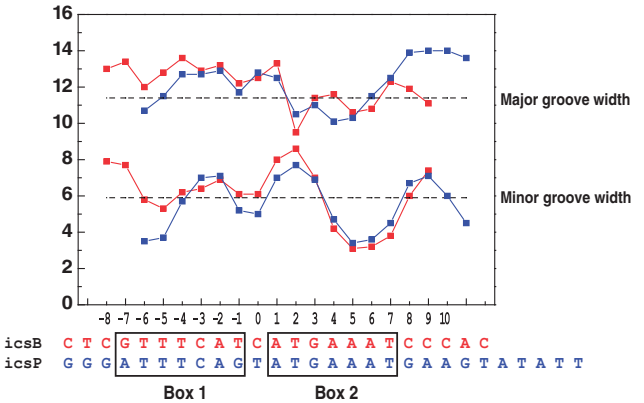

Figure 5. Structural distortion of VirB-bound DNA. Major and minor groove widths for the icsB-wt (red) and icsP-wt (blue) structures. The values are the direct distance between phosphates subtracted by 5.8 Å for the van der Waals radii of the phosphate groups. Dashed lines indicate the groove widths of the standard B-form DNA.

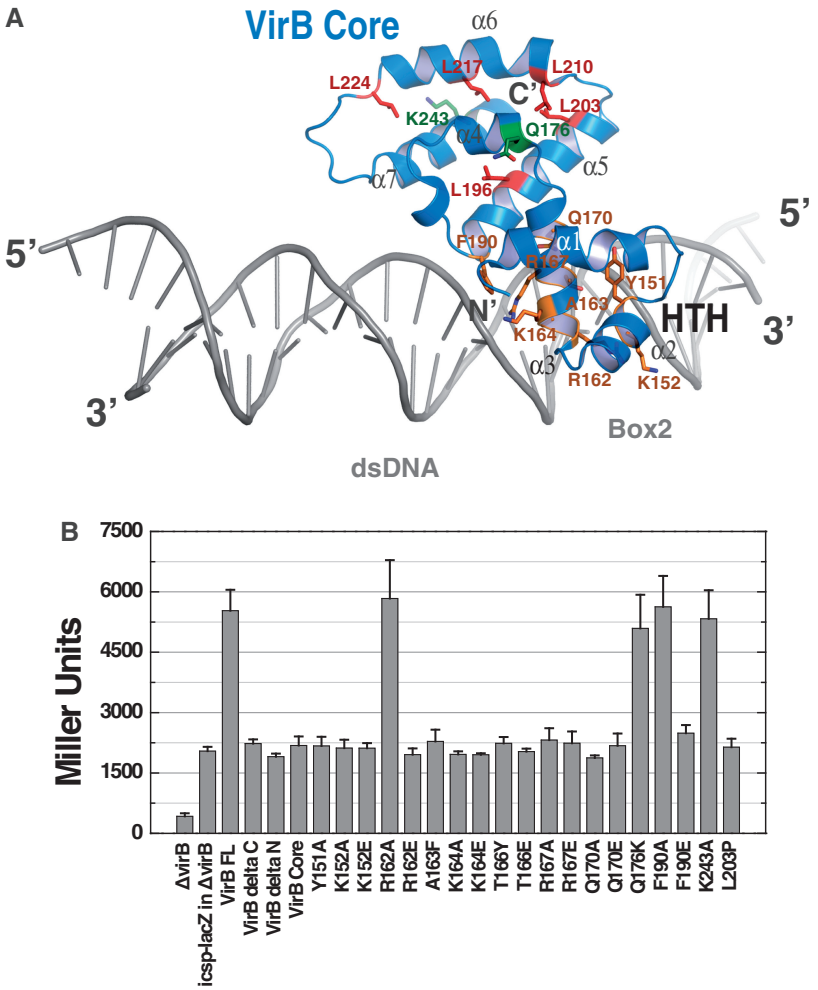

Figure 6. Mutagenesis studies. (**A**) Ribbon diagram of VirB core bound by DNA. Mutations introduced to residues mediating contacts to DNA are colored in orange; to control residues not mediating contacts to DNA are colored in green. Leucine repeats with seven-residue intervals are highlighted in red. (**B**) Activation abilities of VirB mutants and truncations. VirB-dependent promoter activation is assessed by measuring the β-glactosidase activity of icsP-lacZ fusion.

weight of a VirB delta N dimer (41.6 kDa). VirB variants without the C-terminal domain both exist as monomers in solution. The molecular weight calculated for VirB delta C was 26.5 kDa, close to the expected molecular weight of a monomeric VirB delta C (28.5 kDa); the molecular weight calculated for VirB core was 14.0 kDa, matching the expected molecular weight of monomeric VirB core (14.3 kDa). Collectively, our data support that the C-terminal domain of VirB is the determinant for dimer/oligomerization, whereas the N-terminal and the central HTH domain do not mediate dimerization.

Mutagenesis study

Based on structure, we introduced a set of mutations to VirB including mutations at the HTH motif that directly contacts DNA and control mutations at the C-terminal distorted helical bundle that does not bind DNA. We constructed plasmids expressing VirB truncations, VirB delta N, VirB delta C and VirB core. We constructed a VirB mutant L203P that is defective in the transcriptional activation (22), serving the negative control. We then determined the ability of VirB variants and mutants to activate the icsP promoter. Plasmids expressing VirB mutants were transformed to *virB*$^{-}$ *S. flexneri 2a* strain 301 containing an *icsP* promoter fragment (1256 bp upstream of the *icsP* transcription start site) fused to a *lacZ* gene. We conducted the β-galactosidase assays as illustrated in Figure 6A and B. VirB truncations lacking either N- or C-portion or both failed to activate *icsP* promoter controlling the *lacZ* gene because the measured β-galactosidase levels fall to background level as measured for the negative control L203P. Substitutions of the residues involving DNA backbone or base recognition, such as mutants Y151A, K152A, K152E, A163F, K164A, K164E, T166Y, T166E, Q170A and Q170E, lead to the complete losses of VirB-dependent activation; however, exceptions were also found. Although mutation R162E abolished the β-galactosidase activity completely, mutation R162A had no effect at all, indicating that the DNA base contact by R162 side chain is not essential for the activity of VirB. The only essential base contact is provided by R167 because both mutations R167A and R167E abolished the activity to the background level. Mutation F190E abrogated the

VirB-mediated icsP activation, whereas mutation F190A had neglectable effect on the activity. This is likely due to that the backbone NH group of F190 mediates the recognition to DNA backbone by a hydrogen bond that could not be disrupted by mutation F190A. Mutation F190E may lead to the electrostatic repulsion between the glutamic acid and DNA, thus interfering the docking of the HTH domain. Control mutations Q176K, K243A at the C-terminal distorted helical bundle had little effects on the β-galactosidase activity.

DISCUSSION

We determined the crystal structures of the HTH domain of VirB complexed by its cognate sites, demonstrating that VirB is structurally related to the plasmid partitioning proteins. There is no evidence showing that VirB is involved in the existing plasmid partition systems (4,32). Thus, VirB presents a unique example that a protein with ParB-like fold acts exclusively in transcriptional activation. It is reasonable to speculate that VirB might be reassigned to a new regulatory role during evolution; however, the key structural features of its ancestor are preserved. Comparing with the only three available structural studies of ParB-ParS-like complexes, the recognition of the box2 of icsB-wt by VirB HTH domain resembles the recognition of A2-A3 boxes of ParS by ParB HTH domain the most. The recognition of the guanosine bases (third base from 5′ of A-box) by R184 of ParB is preserved in VirB-DNA interactions that the corresponding residue R167 of VirB reads the invariant G_{3c}. R162 of VirB provides another contact to A_{7b} base located at 5′ of box2. However, this contact is not essential for VirB-mediated promoter activation. Thus, R167 is the only residue conferring the DNA sequence specificity.

It was previously predicted that VirB processes a putative leucine zipper domain (190–230 aa) based on the identification of the repeating leucines with 7-residue intervals. The putative leucine zipper mediates the dimer/oligmerization, and the substitution of these leucines negatively affects the dimer/oligomerzation of VirB and its activity *in vivo* (11). Our structures reveal that VirB 175–246 aa region folds into a distorted helical bundle, a structural feature shared with the ParB-like proteins. The structure-based sequence alignment indicates that the C-terminal distorted helical bundle is less conserved compared with that of the HTH motif (Figure 2C), suggesting the subdomain confers the diversity of function among the ParB-like proteins. The structure of VirB shows that the repeating leucines are located on the hydrophobic sides of α5-α6 helices with the side chains wrapped inside the core of the helical bundle, mediating the hydrophobic contacts among the helices (Figure 6A). Therefore, substitutions of these leucines may disrupt the folding of the domain. Our current structural data do not support that the distorted helical bundle of VirB mediates dimer/oligomerization. Interestingly, the structurally equivalent helical bundle in SopB does function as a secondary dimerization domain (19), in which α6-α7 helices mediate the dimer contacts. The α6 helix in VirB contains a kink caused by a proline (P215) in the middle of the helix (Figure 2C); thus, the bent α6 helix cannot support the same type of dimerization as seen in SopB, which requires a straight helix. Beloin *et al.* (22) discovered that mutation P215A did not affect the activity of VirB and the mutant could dimerize more easily than WT VirB *in vivo*. The explanation is likely that the mutation P215A removed the bend and straightened the α6 helix, therefore enabled the α6-α7 helices mediated dimerization.

In the structures of ParB-ParS-like complexes, both half-sites of the inverted repeats are occupied by the HTH domain (19–21). Intriguingly, the structure of VirB-DNA complex show that the HTH domain binds only one half site containing the most matches to the consensus, whereas the other half site is unoccupied. In line with this finding, previous studies have demonstrated that the complete ParS-like site is not essential for VirB-mediated promoter activation, but a close match to the consensus is critical (17,23). On binding by VirB, the box2 of the inverted repeats exhibits the evident conformational deviations. The ability of inducing DNA distortion presents a distinguished role of VirB, which is not shared by other ParB-like proteins because the DNA bound by ParB, KorB or SopB usually adopts the standard B-form DNA conformation. VirB induces a bend at an A-tract segment following the invariant guanine; however, VirB does not provide a specific contact to this segment, and the base contact provided by R162 has been proven not essential for the activity of VirB. It is believed that the A-tract segment is highly flexible and may contain a static bend in solution (33); thus, our data suggest that either the shape or the intrinsic flexibility of the A-tract segment rather than its sequence is recognized by VirB.

The C-terminal domain of VirB shares the least homology with the ParB like proteins. Assuming that VirB was evolved from a ParB analog for plasmid partitioning, while the N-terminal and the HTH domains were well preserved during the evolution, the C-terminal domain might have been diverted to fit its new roles. Previous study showed that the C-terminal of VirB mediates the oligomerization rather than dimerization in a DNA-independent manner, which is essential for its function (22). Our bio-SAXS analyses confirmed that VirB undergoes concentration dependent oligomerization in solution (Supplementary Table S2), which is in accordance with previously reported cross-linking experiments (22). The investigation of oligomerization state of various VirB truncations by size-exclusion chromatography also showed that the C-terminal domain is the determinant for oligomerization. The aforementioned experiments were carried out in the absence of DNA, suggesting that the oligomerization of VirB is independent of DNA binding. Thus, the VirB oligomer may be the functional assembly for DNA binding. In supporting to this hypothesis, our fluorescence study showed that VirB exhibited a clear sign of positive cooperativity in DNA binding that is dependent on the C-terminal domain.

The EMSA results showed that the C-terminal domain of VirB facilitated the assembly of high-ordered VirB-DNA complex, forming a super-shift of huge size. However, this shifted band was efficiently competed by

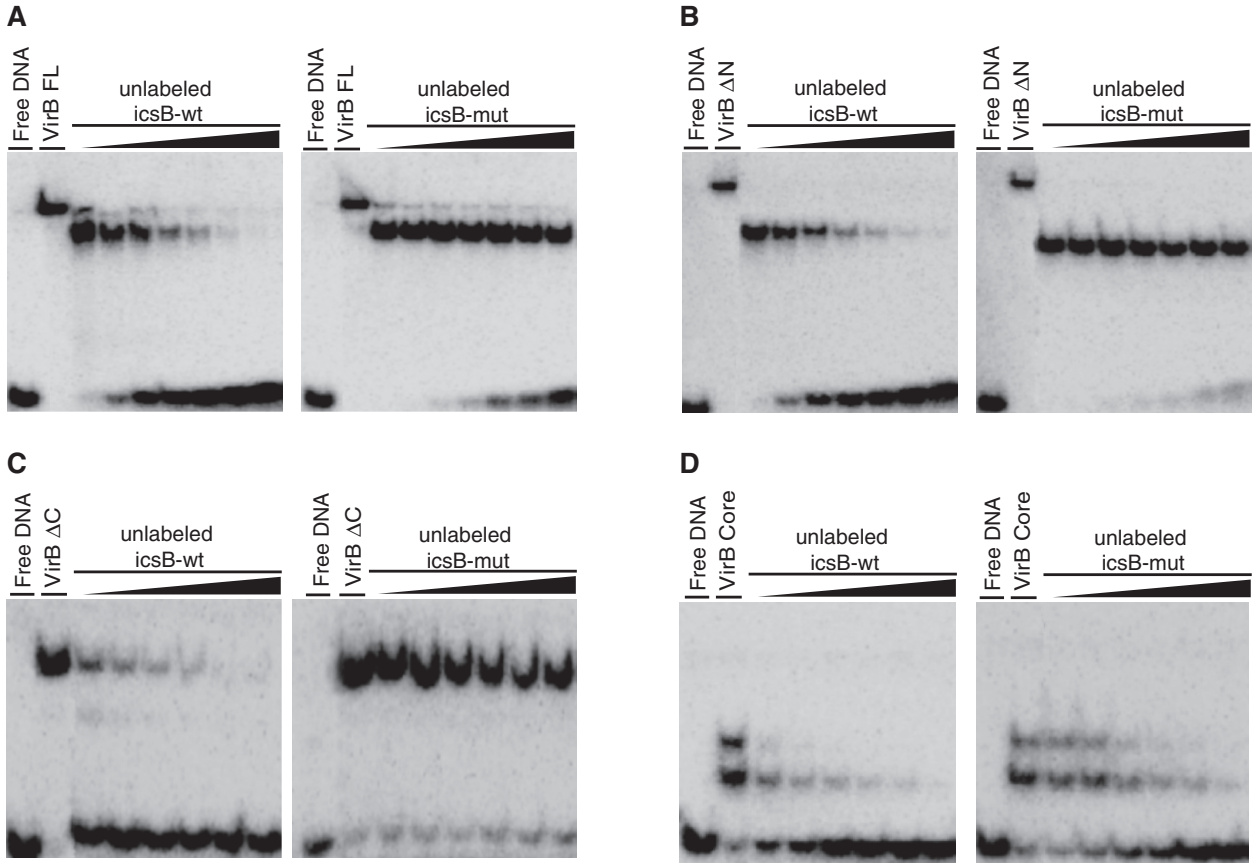

Figure 7. EMSA of VirB variants. EMSAs of the radioactively labeled icsB-wt (2 nM) bound by VirB variants (2 μM): (**A**) VirB FL; (**B**) VirB Delta N; (**C**) VirB Delta C; (**D**) VirB Core. Mixtures of VirB variants, labeled icsB-wt and unlabeled competitor (icsB-wt or icsB-mut as specified) were incubated and resolved by native PAGE, visualized by autoradiography. Each gel in the figure has the same configuration: lane1, free DNA; lane2, VirB variant as indicated; lane 3–8, addition of the increasing amount of unlabeled competitor DNA in 2×, 4×, 8×, 16×, 32× and 64× excess of proteins. Poly dI-dC was included in each reaction to eliminate the non-specific protein–DNA interactions.

icsB-mut, indicating that the formation of the large nucleoprotein complex was mediated by non-specific DNA binding. Surprisingly, a smaller band accumulated when the competitor DNA were added. The band could not be competed with icsB-mut, suggesting a specific VirB-DNA complex. Combining with the results from size-exclusion chromatography, we speculate that the specific VirB-DNA complex might comprise of VirB trimers. VirB core exhibited the least specificity in DNA binding comparing with the other VirB variants, suggesting that isolated HTH domain itself only confers partial DNA specificity; additional determinants for the recognition of the *cis*-acting site may reside in N- or C-terminal domains (Figure 7).

We demonstrate that VirB binds DNA cooperatively, involving both specific and non-specific DNA binding with different affinities. Although the C-terminal portion of VirB is responsible for the assembly of the high-order oligmer, the N-terminal and the central HTH domains contribute to the specific and non-specific DNA binding. Combining these observations, the DNA-binding mode of VirB seems to resemble the model proposed for the DNA binding by the leucine-responsive regulatory protein (Lrp), a regulator of several *E. coli* operons (34). Lrp binds cooperatively to specific or non-specific DNA. The C-terminal domain of Lrp facilitates the oligomerization and is essential for the cooperativity in DNA binding. The initial binding of Lrp dimer to DNA induces a bend, thus enhances the binding to the next Lrp dimer.

In conclusion, our results support and extend a previously proposed model (16,23) for the relieving of H-NS-mediated repression by VirB (Figure 8). The C-terminal domain of VirB facilitates the oligomerization, possibly the trimerization. VirB oligomer acts as the functional assembly for DNA binding. The HTH domain reads the *cis*-acting site upstream the promoter, mediating the initial binding step. The binding by VirB HTH domain induces a bend at the A-tract segment, which assists the subsequent DNA-binding steps, initiating the wrapping of DNA around VirB oligomer. The intrinsic flexibility of the invariant A-tract is likely important to the wrapping of DNA. After the initial binding at the *cis*-acting site, the subsequent DNA binding is mediated by non-specific VirB-DNA interactions. The docking of the first VirB oligomer at the *cis*-acting site serves as a nucleation site that subsequently recruits more VirB oligomers. Thus, VirB polymerizes alone DNA strand (27), forming the large non-specific VirB-DNA complex. The wrapping of

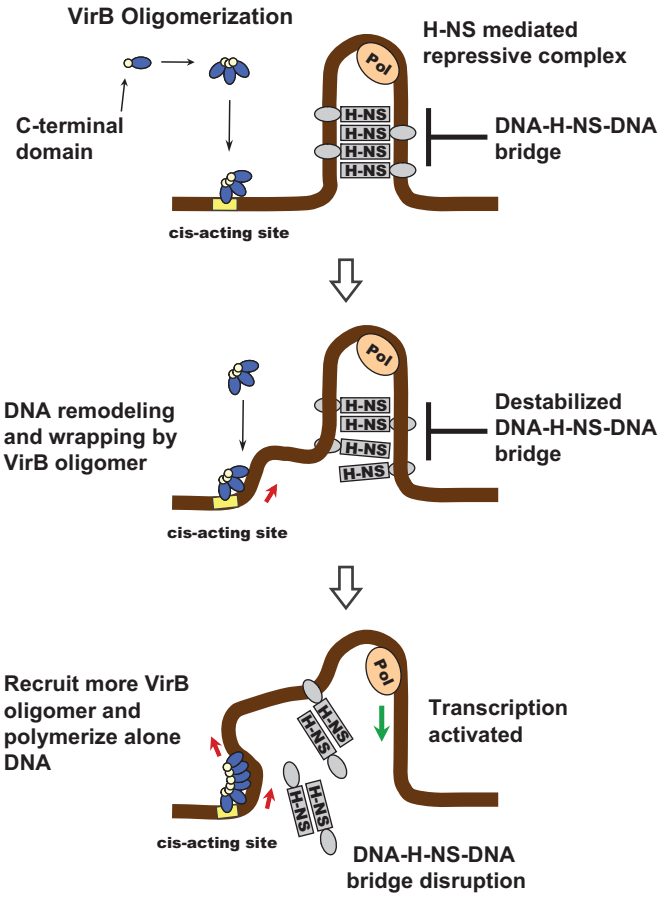

Figure 8. Proposed mechanism for the alleviating of the H-NS mediated transcriptional repression by VirB. The C-terminal domain (yellow) mediates the formation of VirB oligomer (blue). The trimer drawn here represents a given oligomeric form of VirB in solution, possibly trimeric. The HTH domain of VirB recognizes a *cis*-acting site upstream the promoter repressed by H-NS-DNA complex. The binding by the HTH domain induces distortion and bends DNA to initiate DNA wrapping around VirB oligomer. The docking of the first VirB oligomer at the *cis*-acting site serves as a nucleation site that subsequently recruits more VirB oligomer; thus, VirB polymerizes alone the DNA. The DNA remodeling by VirB followed by the spreading of VirB disrupts DNA-N-HS-DNA bridges, leading to the release of the trapped RNA polymerase (orange). The transcription of the virulence gene is de-repressed.

DNA and the polymerization of VirB eventually destabilizes the H-NS-DNA complexes, leading to the collapse of the repressive H-NS-DNA complexes so that the trapped RNA polymerase is released, and the transcription of the virulence genes resumes.

ACCESSION CODES

The atomic coordinates and structure factors have been deposited in the Protein Data Bank with the accession codes 3VWB, 3W3C and 3W2A.

SUPPLEMENTARY DATA

Supplementary Data are available at NAR Online.

ACKNOWLEDGEMENTS

The authors thank Swiss Light Source (SLS) PX beamlines and Shanghai Synchrotron Radiation Facility (SSRF) beamline BL17U for beam time allowance and help with data collection. The authors X.G. and T.Z. contributed equally for this work.

FUNDING

National Basic Research Program of China (973 Program) [2011CB504900]; National Science and Technology Major Project [2013ZX10004601]; the Fundamental Research Funds for the Central Universities [2012N02]; and Specialized Research Fund for the Doctoral Program of Higher Education [20121106110048]. Funding for open access charge: National Basic Research Program of China (973 Program) [2011CB504900].

Conflict of interest statement. None declared.

REFERENCES

1. Hacker,J. and Kaper,J.B. (2000) Pathogenicity islands and the evolution of microbes. *Annu. Rev. Microbiol.*, **54**, 641–679.
2. Yang,F., Yang,J., Zhang,X., Chen,L., Jiang,Y., Yan,Y., Tang,X., Wang,J., Xiong,Z., Dong,J. *et al.* (2005) Genome dynamics and diversity of Shigella species, the etiologic agents of bacillary dysentery. *Nucleic Acids Res.*, **33**, 6445–6458.
3. Sansonetti,P.J. (2006) Shigellosis: an old disease in new clothes? *PLoS Med.*, **3**, e354.
4. Buchrieser,C., Glaser,P., Rusniok,C., Nedjari,H., D'Hauteville,H., Kunst,F., Sansonetti,P. and Parsot,C. (2000) The virulence plasmid pWR100 and the repertoire of proteins secreted by the type III secretion apparatus of Shigella flexneri. *Mol. Microbiol.*, **38**, 760–771.
5. Jin,Q., Yuan,Z., Xu,J., Wang,Y., Shen,Y., Lu,W., Wang,J., Liu,H., Yang,J., Yang,F. *et al.* (2002) Genome sequence of Shigella flexneri 2a: insights into pathogenicity through comparison with genomes of Escherichia coli K12 and O157. *Nucleic Acids Res.*, **30**, 4432–4441.
6. Le Gall,T., Mavris,M., Martino,M.C., Bernardini,M.L., Denamur,E. and Parsot,C. (2005) Analysis of virulence plasmid gene expression defines three classes of effectors in the type III secretion system of Shigella flexneri. *Microbiology*, **151**, 951–962.
7. Porter,M.E. and Dorman,C.J. (1994) A role for H-NS in the thermo-osmotic regulation of virulence gene expression in Shigella flexneri. *J. Bacteriol.*, **176**, 4187–4191.
8. Bouffartigues,E., Buckle,M., Badaut,C., Travers,A. and Rimsky,S. (2007) H-NS cooperative binding to high-affinity sites in a regulatory element results in transcriptional silencing. *Nat. Struct. Mol. Biol.*, **14**, 441–448.
9. Dame,R.T., Noom,M.C. and Wuite,G.J. (2006) Bacterial chromatin organization by H-NS protein unravelled using dual DNA manipulation. *Nature*, **444**, 387–390.
10. Schröder,O. and Wagner,R. (2000) The bacterial DNA-binding protein H-NS represses ribosomal RNA transcription by trapping RNA polymerase in the initiation complex. *J. Mol. Biol.*, **298**, 737–748.
11. Dame,R.T., Wyman,C., Wurm,R., Wagner,R. and Goosen,N. (2002) Structural basis for H-NS-mediated trapping of RNA polymerase in the open initiation complex at the rrnB P1. *J. Biol. Chem.*, **277**, 2146–2150.
12. Porter,M.E. and Dorman,C.J. (1997) Differential regulation of the plasmid-encoded genes in the Shigella flexneri virulence regulon. *Mol. Gen. Genet.*, **256**, 93–103.
13. Dorman,C.J., McKenna,S. and Beloin,C. (2001) Regulation of virulence gene expression in Shigella flexneri, a facultative intracellular pathogen. *Int. J. Med. Microbiol.*, **291**, 89–96.

14. Porter,M.E. and Dorman,C.J. (2002) *In vivo* DNA-binding and oligomerization properties of the Shigella flexneri AraC-like transcriptional regulator VirF as identified by random and site-specific mutagenesis. *J. Bacteriol.*, **184**, 531–539.
15. Tobe,T., Yoshikawa,M., Mizuno,T. and Sasakawa,C. (1993) Transcriptional control of the invasion regulatory gene virB of Shigella flexneri: activation by virF and repression by H-NS. *J. Bacteriol.*, **175**, 6142–6149.
16. Kane,K.A. and Dorman,C.J. (2011) Rational design of an artificial genetic switch: Co-option of the H-NS-repressed proU operon by the VirB virulence master regulator. *J. Bacteriol.*, **193**, 5950–5960.
17. Turner,E.C. and Dorman,C.J. (2007) H-NS antagonism in Shigella flexneri by VirB, a virulence gene transcription regulator that is closely related to plasmid partition factors. *J. Bacteriol.*, **189**, 3403–3413.
18. Lee,D.J., Minchin,S.D. and Busby,S.J. (2012) Activating transcription in bacteria. *Annu. Rev. Microbiol.*, **66**, 125–152.
19. Schumacher,M.A., Piro,K.M. and Xu,W. (2010) Insight into F plasmid DNA segregation revealed by structures of SopB and SopB-DNA complexes. *Nucleic Acids Res.*, **38**, 4514–4526.
20. Khare,D., Ziegelin,G., Lanka,E. and Heinemann,U. (2004) Sequence-specific DNA binding determined by contacts outside the helix-turn-helix motif of the ParB homolog KorB. *Nat. Struct. Mol. Biol.*, **11**, 656–663.
21. Schumacher,M.A. and Funnell,B.E. (2005) Structures of ParB bound to DNA reveal mechanism of partition complex formation. *Nature*, **438**, 516–519.
22. Beloin,C., McKenna,S. and Dorman,C.J. (2002) Molecular dissection of VirB, a key regulator of the virulence cascade of Shigella flexneri. *J. Biol. Chem.*, **277**, 15333–15344.
23. Kane,K.A. and Dorman,C.J. (2012) VirB-mediated positive feedback control of the virulence gene regulatory cascade of Shigella flexneri. *J. Bacteriol.*, **194**, 5264–5273.
24. Taniya,T., Mitobe,J., Nakayama,S., Mingshan,Q., Okuda,K. and Watanabe,H. (2003) Determination of the InvE binding site required for expression of IpaB of the Shigella sonnei virulence plasmid: involvement of a ParB boxA-like sequence. *J. Bacteriol.*, **185**, 5158–5165.
25. Castellanos,M.I., Harrison,D.J., Smith,J.M., Labahn,S.K., Levy,K.M. and Wing,H.J. (2009) VirB alleviates H-NS repression of the icsP promoter in Shigella flexneri from sites more than one kilobase upstream of the transcription start site. *J. Bacteriol.*, **191**, 4047–4050.
26. Schumacher,M.A., Mansoor,A. and Funnell,B.E. (2007) Structure of a four-way bridged ParB-DNA complex provides insight into P1 segrosome assembly. *J. Biol. Chem.*, **282**, 10456–10464.
27. McKenna,S., Beloin,C. and Dorman,C.J. (2003) *In vitro* DNA-binding properties of VirB, the Shigella flexneri virulence regulatory protein. *FEBS Lett.*, **545**, 183–187.
28. Datsenko,K.A. and Wanner,B.L. (2000) One-step inactivation of chromosomal genes in Escherichia coli K-12 using PCR products. *Proc. Natl Acad. Sci. USA*, **97**, 6640–6645.
29. Heck,H.D. (1971) Statistical theory of cooperative binding to proteins. The Hill equation and the binding potential. *J. Am. Chem. Soc.*, **93**, 23–29.
30. Holm,L. and Sander,C. (1993) Protein structure comparison by alignment of distance matrices. *J. Mol. Biol.*, **233**, 123–138.
31. Lavery,R. and Sklenar,H. (1988) The definition of generalized helicoidal parameters and of axis curvature for irregular nucleic acids. *J. Biomol. Struct. Dyn.*, **6**, 63–91.
32. Radnedge,L., Davis,M.A., Youngren,B. and Austin,S.J. (1997) Plasmid maintenance functions of the large virulence plasmid of Shigella flexneri. *J. Bacteriol.*, **179**, 3670–3675.
33. Stella,S., Cascio,D. and Johnson,R.C. (2010) The shape of the DNA minor groove directs binding by the DNA-bending protein Fis. *Genes Dev.*, **24**, 814–826.
34. Peterson,S.N., Dahlquist,F.W. and Reich,N.O. (2007) The role of high affinity non-specific DNA binding by Lrp in transcriptional regulation and DNA organization. *J. Mol. Biol.*, **369**, 1307–1317.